

Functional Properties of Biodegradable Nanocomposites from Poly Lactic Acid (PLA)

Saeed Dadashi^{1*}, Seyed Mohammad Mousavi¹, Zahra Emam-Djomeh¹, Abdulrasoul Oromiehie²

1. Department of Food Science, Engineering and Technology, Faculty of Agricultural Engineering & Technology, College of Agriculture & Natural Resources, University of Tehran, Karaj, I.R Iran
2. Iran Polymer and Petrochemical Institute, Pazhoohesh Street, Tehran, I.R Iran

(*) Corresponding author: Dadashis@ut.ac.ir

(Received: 24 Oct. 2012 and accepted: 23 Nov. 2014)

Abstract:

Nanocomposite composed of organoclay (Cloisite 20A-C20A) and Poly lactic acid (PLA) was prepared by solvent casting method. Physical, mechanical, thermal, barrier and microstructure properties of the composite were studied. X-Ray diffraction (XRD) patterns and scanning electron microscopy (SEM) images revealed that the diffraction peak of nanoclay shifted to lower angles and the *d*-spacing between the C20A layers increased. The formation of an intercalated structure with good compatibility and homogeneously dispersed nanoparticles was observed. Tensile strength (TS) and elastic modulus (E-M) of PLA/C20A nanocomposites increased significantly with clay concentrations, while the values of elongation (E) percentage decreased dramatically. Glass transition temperature (T_g) and degree of crystallinity ($\chi\%$) were determined by DSC (Differential Scanning Calorimetry). The presence of C20A provoked significant raise in both the T_g and the degree of crystallinity. The water vapor permeability (WVP) of the nanocomposites compared to pure PLA moved down by approximately 12-50% by adding 3-7 wt% C20A. An atomic force microscopy (AFM) was applied to evaluate the surface morphology and roughness of PLA films. Pure PLA possessed smoother surfaces and a lower roughness parameter (Sa). New composite based on PLA and C20A could prove to be an improved biopolymer with better functional properties for packaging and other applications.

Keywords: Nanocomposite, Nanoparticle, Functional properties, PLA, Packaging.

1. INTRODUCTION

The use of biopolymers has been increasing due to more environmentally aware consumers, increased price of crude oil and the concern about global warming [1,2]. Biopolymers are naturally occurring polymers that are found in all living organisms. The use of biopolymers will have a less harmful effect on our environment compared to the use of fossil fuel based commodity plastics [3]. The most popular and important biodegradable polymers are aliphatic polyesters, such as

Polylactic acid (PLA), Polycaprolactone (PCL), Poly (3-hydroxybutyrate) (PHB), and Polyglycolic acid (PGA) [4]. They are used in bone fracture fixtures, drug delivery systems, wound dressings, and packaging applications [5]. PLA as a linear aliphatic thermoplastic polyester produced from renewable resources has received much attentions [6,7], which is produced either by ringopening polymerization of lactide or by polycondensation of the lactic acid monomers, and the monomer is obtained from the fermentation of corn or other renewable agricultural raw resources [8, 9]. PLA is

becoming increasingly popular as a biodegradable plastic owing to its high mechanical strength and easy processability compared to other biopolymers [10]. The main limitations of this biodegradable polymer are its poor thermal and mechanical resistance and limited gas barrier properties compared to petroleum based polymers, which limit its applications in industrial sectors, such as packaging [11].

The above drawbacks could be overcome by enhancing their thermomechanical properties through copolymerization, blending and filling techniques. Indeed, the addition of nano-sized fillers would potentially confer multifunctional enabling properties to these polymers [12,13]. Nanocomposites are a new class of composites that are particle-filled polymers for which at least one dimension of the dispersed particles is in the nanometer range. Nanocomposites are considered as the materials of the 21st century and it is expected that they will be used more and more intensively in future years [14,15].

The first research on polymer based nanocomposites was done by researchers at Toyota company in Japan in the early 1990s [16]. In this research, layered silicates were used as nanoreinforcements and have received wide attention after this work. Recently, nano-scale composites of PLA with various nanofillers have been studied extensively. Pluta et al. (2002) [17], investigated PLA/MMT micro and nanocomposites that prepared by melt intercalation technique, and showed that the microcomposites have formed a phase-separation between the matrix and reinforcement. Furthermore, nanocomposites can be very easily processed by using nanofillers; however, the biodegradability of the composite was affected. Moreover, the thermal stability in oxidative atmosphere of PLA/MMT could be improved. Lewitus et al. (2006) [47], used organically modified montmorillonite clays to preparing PLA/clay nanocomposites with using a single screw cast film extruder. The thermal and mechanical properties of the films were examined in order to determine the effect of the clay and different carriers on the polymer-clay interactions. In the optimal case, the tensile modulus increased by 30 %, elongation increased by 40 %, and the

cold crystallization temperature decreased by 15 °C, compared to neat PLLA. In a study done by Rhim et al. (2009) [19], PLA-based composite films with different types of nanoclays, including: Cloisite Na⁺, Cloisite 30B and Cloisite 20A, were prepared and their mechanical, water vapor permeability and antimicrobial properties were tested. According to their results, water permeability of the nanocomposite decreased 6-33 % through nanoclay compounding. Among the clay types used, Cloisite 20A was the most effective one in improving the water vapor barrier property while sacrificing tensile properties the least, also only PLA/Cloisite 30B composite film showed a bacteriostatic function against *Listeria monocytogenes*. Harinatharavimal et al. (2010) [18], developed a toughened polylactic acid (PLA) nanocomposite and investigated the effects of linear low density polyethylene (LLDPE) and MMT on properties of PLA. The Young's and flexural modulus improved, the crystallization temperature and glass transition temperature dropped gradually while the thermal stability of PLA improved with increasing content of MMT. Chiang et al. (2012) [8], reported the preparation and physical properties of biodegradable nanocomposites fabricated using poly (L-lactide) (PLLA) and γ -polyglutamate-modified magnesium/aluminum layered double hydroxide (γ -LDH). Mechanical properties of the fabricated 5 wt% PLLA/ γ -LDH nanocomposites show significant enhancements in the storage modulus when compared to neat PLLA.

There are few studies in which in the same condition all of the properties of PLA and its nanocomposites have been evaluated. Some of them, such as the above-mentioned, have studied only physical or mechanical or thermal properties. In this study, we attempted to do a comprehensive assessment of the functional properties of produced nanocomposites. Therefore, the aim of this study was the preparation and characterization of PLA films and their nanocomposites with layered silicate nanoparticles. Also the influence of layered silicate loading on the phase morphology, the dispersion of nanoparticles, physical, mechanical, thermal and barrier properties of the resulting PLA/layered silicate nanocomposite films were investigated in details.

2. MATERIALS AND METHODS

2.1. Materials

Key materials to carry out experimental tests were mainly as follows:

PLA (Bio-flex[®]F 6510) was provided from FKUR Kunststoff GmbH Siemensring 79, Germany, with a density of 1300 kg/m³, melting point of 150-170 °C and molecular weight (M_w) of 197000 g/mol. PLA resins were dried in a vacuum oven at 60 °C for 24 hours before use. Organically modified montmorillonite (Cloisite 20A; C20A), as nanoreinforcement, was supplied from Southern Clay (Gonzales, TX, USA). Chloroform (Merck Chemicals Co. Darmstadt, Germany) was used to dissolve PLA and to swell and disperse nanoreinforcement clay. Silicon 100 was used to grease the molds prior to casting.

2.2. Preparation of films

PLA and PLA-based nanocomposite films were prepared using a solvent casting method and according to the method described by Rhim et al. (2009) [19], with some modifications. Five grams of PLA was dissolved in 100 mL of chloroform while agitating vigorously for 8 hours at room temperature (25°C). The dissolved solution was poured onto greased glass molds and then allowed to dry for about 24 hours at room temperature. The manufactured film was removed from the casting surface. For the preparation of PLA nanocomposite films, a predetermined amount of C20A was dispersed in the solvent by vigorous stirring for 8 hours with a magnetic stirrer. They were then homogenized at 8,000 rpm for 15 min in an ultraturax T-25 homogenizer (IKA T25-digital ultraturax, Staufen, Germany) with a S25N-25F probe, followed by sonication for 30 min at room temperature by a high intensity ultrasonic processor (Model VCX 750, Sonics & Materials Inc., Newtown, CT, USA). The nanoclay solutions were mixed with the previously prepared PLA solution and then stirred for 15 min with a magnetic stirrer. The solutions were homogenized at 8,000 rpm for 15 min and sonicated for another 30 minutes, then casted onto greased glass molds.

The final film was obtained by the same procedure explained above for pure PLA films. The effect of the C20A content was tested with PLA/C20A films prepared with different nanoclay percentages, i.e., 0, 3, 5, and 7 (wt%) of the nanoclay. After drying at room temperature for 24 hours, all PLA films were further dried at 60°C in a vacuum dryer to remove the remaining solvent (chloroform) to prevent its plasticizing effect [20].

2.2. Physical properties

2.2.1. Film thickness

Thickness of the films was measured by means of a digital Magna-Mike (Magna-Mike Model 8000, USA) to the nearest 0.001 mm. Measurements were performed when the magnetic probe was held against one side of the test film and a small steel target ball was placed on the opposite side. The probe's Hall Effect sensor measures the distance between the probe tip and the ball, and then displays it as a digital thickness reading. Measurements were made in at least ten random locations for each film, and an average value was reported.

2.2.2. Transmittance

Film transparency was determined by lux meter (Testo 540 pocket sized lux meter, UK).

2.2.3. Surface color

Visual color was detected with a Minolta colorimeter (Minolta CR 300 Series, Minolta Camera Co., Ltd., Osaka, Japan), in terms of L (lightness), a (redness and greenness), and b (yellowness and blueness). The instrument (45/0 geometry, 10 observer) was calibrated with a standard white tile ($L^* = 93.49$, $a^* = -0.25$, $b^* = -0.09$). L values range from 0 (black) to 100 (white); a values range from -80 (greenness) to 100 (redness); and b values range from -80 (blueness) to 70 (yellowness). All measurements were performed in triplicates.

2.3. XRD pattern

XRD patterns were obtained from X'Pert MPD, Philips Co, Holland X-ray diffractometer equipped with radiation Co K α beam at a voltage of 40 kV and current of 30 mA. The relative intensity was recorded at ambient temperature over an angular range (2θ) of 2-45° at a rate of 1°/min and a step size of 0.02. The samples were cut in 7 × 12 mm² rectangles and placed on a glass plate, and the set was placed inside the chamber of the apparatus for measurement.

2.4. Mechanical properties

Testometric Machine M350-10CT (Testometric Co. Ltd., Rochdale, Lancs., England) was applied to study the mechanical properties of the film samples upon the guidelines of ASTM standard method D882 (1996) [22]. Initial grip separation was set at 50 mm and cross-head speed at 50 mm/min. Tensile strength (TS) was calculated by dividing the maximum load on the film before failure by the cross-sectional area of the initial specimen. Elastic modulus (E-M) was determined according to the slope of the stress /strain curve in the linear range. Percentage elongation (E) was defined as the percentage change in the length of the specimen to the original length between the grips. At least five replicates of each film were tested.

2.5. Thermal characteristics

Thermal behavior of the specimens was evaluated by DSC (DSC Pyris 6, Perkin Elmer Co. USA). Samples of 2-4 mg were sealed in standard aluminum dishes, using a sealed empty aluminum dish as the reference sample. Experiments were conducted from -10 to 200 °C, with a heating rate of 10 °C/min, on all of the samples. Degree of crystallinity (χ_c) was calculated by using a value of 93 J/g for the heat of fusion of the 100% crystalline PLA [21].

2.6. Water vapor permeability

Water vapor permeability (WVP) was measured gravimetrically according to the standard method

E96 (ASTM Standards, 1995) [23] and similar to that manipulated by Ghasemlou et al. (2011) [24] and corrected for the stagnant air gap inside test cups according to the equations of Gennadios et al. (1994) [25]. Special glass cups with wide rims were used to determine WVP. The cups, contained approximately 80 g of anhydrous calcium chloride desiccant (0 % RH, assay cup) or nothing (control cup), were covered with different films. Films without pinholes or defects were cut circularly (0.002827 m² film area) and sealed to the cup mouths using molten paraffin. Each cup was placed in desiccators and maintained at 75 % RH with a sodium-chloride-saturated solution. This difference in RH corresponds to a driving force of 1753.55 Pa, expressed as water vapor partial pressure. After the films were mounted, the weight gain of the whole assembly was recorded every 1 hour during the first 9 hours and finally after 24 hours (with an accuracy of 0.0001 g). The cups were shaken horizontally after every weighing. The slope of the weight versus time plot (the lines' regression coefficients were >0.998) was divided by the effective film area to obtain the water vapor transmission rate. This was multiplied by the thickness of the film and divided by the pressure difference between the inner and outer surfaces to obtain the WVP (Eq.1).

$$WVP = \frac{\Delta m \cdot X}{A \Delta t \Delta P} \quad (1)$$

where $\Delta m/\Delta t$ is the weight of moisture gain per unit of time (gS⁻¹), X is the average film thickness (m), A is the area of the exposed film surface (m²), and ΔP is the water vapor pressure difference between the two sides of the film (Pa). WVP was measured for three replicated samples for each type of film.

2.7. Film microstructure

Film microstructure was determined by scanning electron microscopy (SEM) (Philips-XL30, Rotterdam, Netherlands). Samples were prepared using standard techniques, mounted on aluminum tubs, and sputter coated with gold (100 Å) (Gounga et al., 2007). The micrographs were collected using an accelerating voltage of 25-30 kV.

2.8. Atomic force microscopy

The surface morphology of the films that had been previously equilibrated at 50 % RH was studied using atomic force microscopy (AFM) (Duals cope/Raster scope C26, DME, Denmark) with a 200 $\mu\text{m} \times 200 \mu\text{m}$ scan size and a 6 μm vertical range. Samples were cut into thin pieces that fit into AFM imaging, and were stuck onto the sample stage by double-sided tape and scanned in noncontact mode. A sharpened cantilever with a spring constant of 25 N/m was positioned over the sample, and 50 $\mu\text{m} \times 50 \mu\text{m}$ images were obtained. The resulting data for each sample was transformed into a 3D image [24]. To make the results comparable, the images were obtained from the centre area of each surface. Three images of different zones were examined and analyzed offline with Duals cope/Raster scope SPM software (Version 2.1.1.2) to calculate the roughness value. Various roughness parameters can be measured by AFM. In this study we calculated the average roughness (S_a), root mean square (rms) roughness (S_q) and the slope for each point of area excluding points on the edge (S_{dq}).

2.9. Statistical analysis

Statistics on a completely randomized design were performed with the analysis of variance (ANOVA) procedure using SAS software (version 9.1; Statistical Analysis System Institute Inc., Cary, NC, USA). Duncan's multiple range tests were used to compare the difference among mean values at the confidence level of 0.95 ($P=0.05$).

3. RESULTS AND DISCUSSION

3.1. Physical properties

Table 1 shows the effects of incorporating C20A

on the physical properties of PLA films. The thickness of pure PLA film was 80.20 μm and increased to 82.51, 82.62 and 83.05 μm with addition 3, 5 and 7 percentage (wt%) of C20A respectively. Since the distribution of C20A in the chloroform, swelling it and the space between plates increase, this increase in the thickness of the films was expectable. However, the film thickness can be influenced by changing amounts of components (adding the nanoclay), while the casting area is the same.

Figures 1 shows the optical clarity of the nanocomposite materials. This image and table 1 show that the incorporation of C20A in PLA matrix doesn't have any significant effects on films transparency. In general, the optical property of a well-developed nanocomposite film does not change significantly when the clay platelets with about 1 nm thickness are well dispersed through the polymer matrix, since such clay platelets with sizes less than the wavelength of visible light do not hinder light's passage [26]. However, the large decrease in the transmittance of the composite films indirectly indicates that the clays are not completely dispersed in the polymer matrix. Another possible reason for the decreased transparency of the composite films is due to the probable crystallization of solvent cast PLA films [19].

Film color is an important factor in a product's acceptability by consumers. Effect of the addition of nanoparticles on color parameters of PLA-based nanocomposites is presented in Table 1. L parameter did not change significantly with increasing C20A content and was about 56.25 for nanocomposite with 3% nanoclay and 56.69 for pure PLA. While, a parameter reduced, in other words, the red color value of samples decreased and green color value increased. b parameter did not show regular changes. These results can be attributed to the nature of C20A and also agreed with visual observations.

Table 1. Physical properties of PLA film and its nanocomposites

Composition	Thickness (μm)	Transparency (%)	Color parameters		
			L	a	b
PLA	80.20 \pm 4.07 ^b	85.86 \pm 1.97 ^a	56.69 \pm 1.26 ^a	-0.11 \pm 0.07 ^a	-3.08 \pm 0.09 ^c
PLA/3%C	82.51 \pm 2.48 ^{ab}	84.23 \pm 1.04 ^{ab}	56.32 \pm 2.32 ^a	-0.21 \pm 0.02 ^b	-2.09 \pm 0.06 ^a
PLA/5%C	82.62 \pm 4.40 ^{ab}	83.71 \pm 1.29 ^b	56.48 \pm 0.62 ^a	-0.29 \pm 0.02 ^c	-2.39 \pm 0.06 ^b
PLA/7%C	83.05 \pm 3.97 ^a	83.80 \pm 0.86 ^{ab}	56.25 \pm 1.23 ^a	-0.28 \pm 0.04 ^c	-2.41 \pm 0.08 ^b

^{a,b,c} Letters indicate the statistical difference in column (between samples).

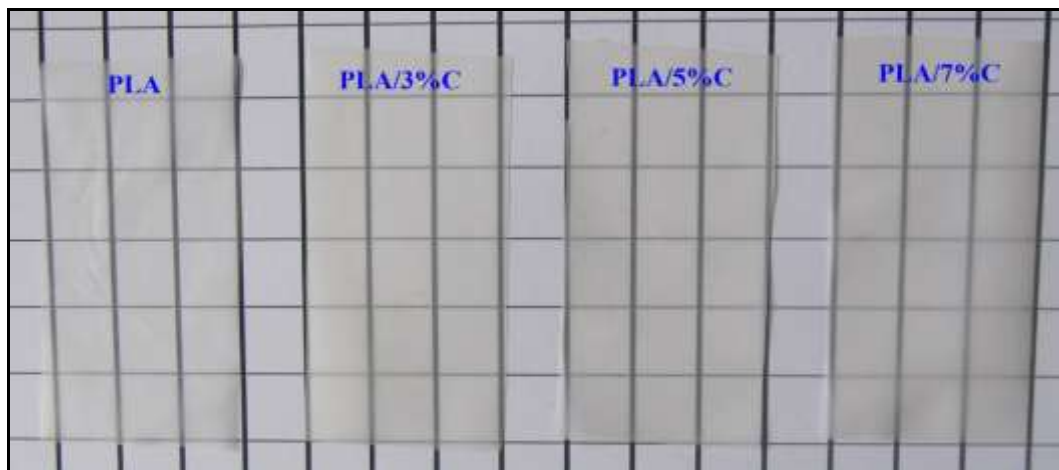


Figure 1. Comparison of pure PLA and nanocomposites containing C20A appearance

3.2. XRD patterns

The pure PLA, C20A and nanocomposites based on PLA were characterized by X-ray diffraction to study the effect of incorporation of nanoreinforcement and its content on the structure and crystallinity of PLA. X-ray diffraction results are shown in Figures 2. The amorphous region presented the broad scattered region, while the crystalline region showed a typical sharp diffraction peak pattern. As can be seen in Figures 2, the pure PLA have X-ray diffraction peaks at $2\theta = 12.56, 22.44, 25.50, 38.67$ and 39.75 . Also C20A have a peak at $2\theta = 4.25^\circ$. These results indicate that the structure of pure PLA is semi-crystalline. Pure PLA in the range of 2-10 has no peak and in most previous studies, this region has been investigated [19, 27, 28]. Incorporation of C20A in polymer matrix causes an increase in intensity and sharpness of PLAs peaks, which can be attributed to improvement of matrix crystallinity. When C20A are combined with PLA, its peak in 4.25° did not appear in Figures 2, but when the region of 2- 10° is magnified (Figures 3), two weak peaks can be seen at 3.76 and 3.84° for nanocomposites with 5% and 7% C20A, respectively. According to the Bragg diffraction equation: $2d\sin\theta = \lambda$, the d-spacing between the C20A layers in pure C20A and nanocomposites with 5% and 7% C20A are 2.41, 2.72 and 2.67nm, respectively. These results indicate that most of the clays are intercalated by ultra-turrax and

ultrasound during the processing and polymer chains diffused of through the clay layers and forming intercalated nanocomposite, without reaching complete exfoliation. These results are in good agreement with those previously reported [19, 27, 28]. As can be seen in Figure 3, sample with 3% C20A does not show any diffraction peak. According to Sinha et al. (2005) [34], in the case of exfoliated structures, there is no peak in XRD patterns, indicating polymer chains have penetrated the gallery and clay clusters lose their layered identity and are well separated into single sheets within the continuous polymer phase. This is due to a high affinity between polymer and clay. So in this case, there is the possibility of exfoliated structure. However, in this case additional tests such as TEM (Transmission Electron Microscopy) are needed to prove exfoliated structure. Since the major portion of the nanocomposite films consists of the biopolymer matrix, the similar pattern of XRD was observed in all the nanocomposite films with different C20A concentration, whereas only the intensity of the diffraction peaks varied.

3.3. Mechanical properties

Mechanical properties reflect the durability of films and their ability to enhance the mechanical integrity of foods. In Figures 4 and 5 the Mechanical properties of PLA/C20A nanocomposite films with various clay content resulted from the tensile test are shown. The mechanical properties were significantly ($P < 0.05$) influenced with the amount of clay addition and

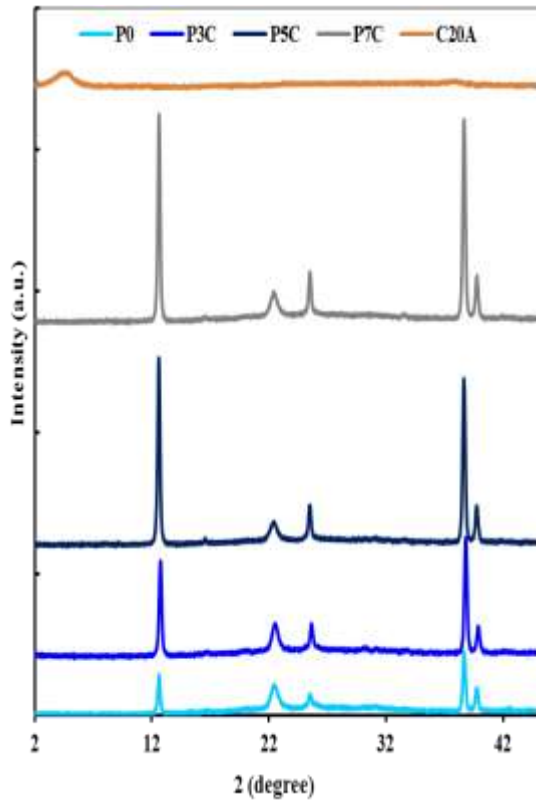


Figure 2. XRD patterns of pure PLA, C20A and nanocomposites containing C20A

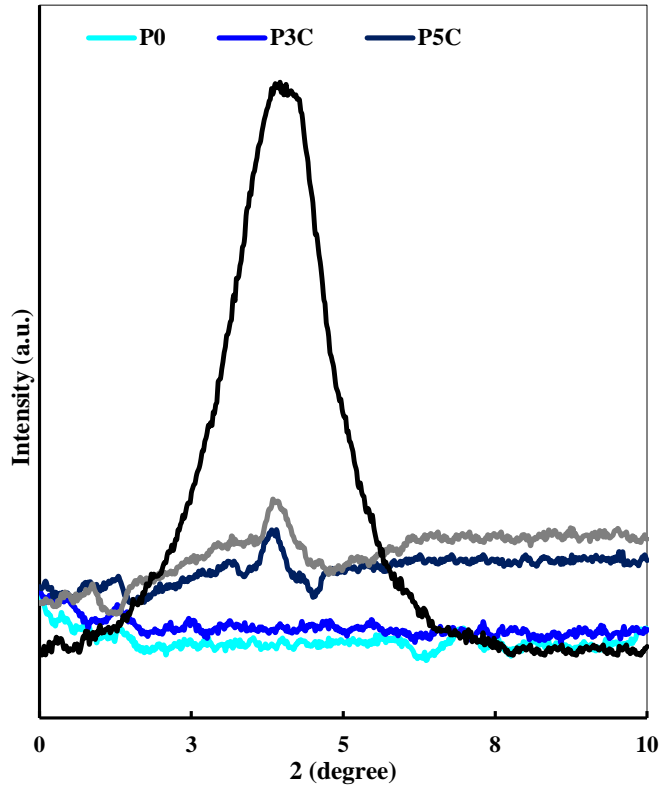


Figure 3. XRD patterns of pure PLA, C20A and nanocomposites containing C20A in range of 2-10 (2θ)

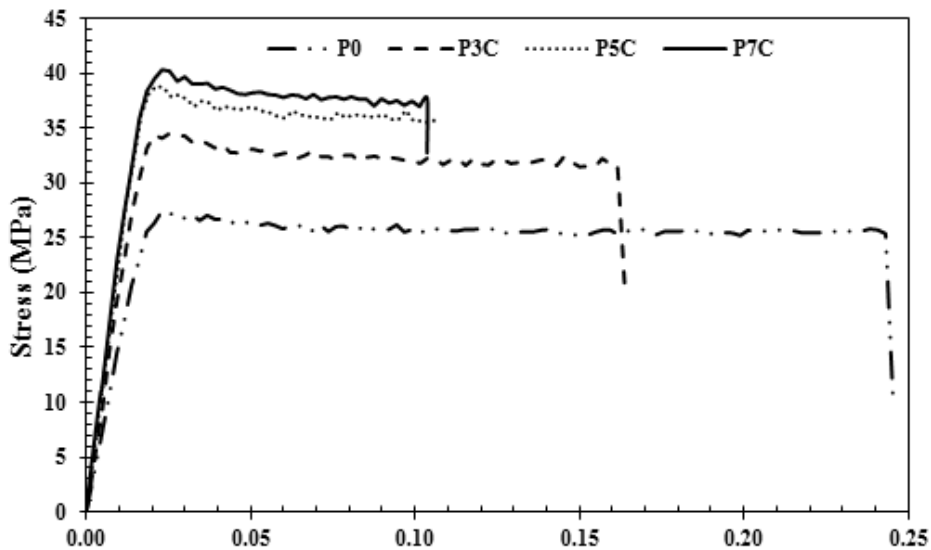


Figure 4. Stress-strain curves of pure PLA and nanocomposites

C20A acts as a mechanical reinforcement of polymer reducing the flexibility of the polymer. Films without C20A presented greater E (24.53 %) and lower TS (27.44 MPa) and E-M (1.84 GPa). As can be seen, the addition of 7% of C20A to PLA increased the TS and E-M of the

nanocomposites by 47% and 42%, respectively, while E decreased 58 %. These findings are consistent with previous studies [18, 19, 29, 30] which reported similar enhancement in terms of mechanical properties with incorporation of MMT. The improvement in mechanical properties was

due to the reinforcement effect of the rigid inorganic C20A which constrains the molecular motion of PLA chains. The main reason for this behavior may be attributed to the resistance exerted not only by the clay itself with high surface area, high aspect ratio, and very high elastic modulus [31, 32, 33, 34, 35], but also by the stronger interfacial interaction between the matrix and layered silicate due to the vast surface exposed to the clay layers. During the processing and drying of the composites, the original hydrogen bonds formed between the PLA molecules and the C20A. The existence of these new hydrogen bonds would improve the mechanical properties [36].

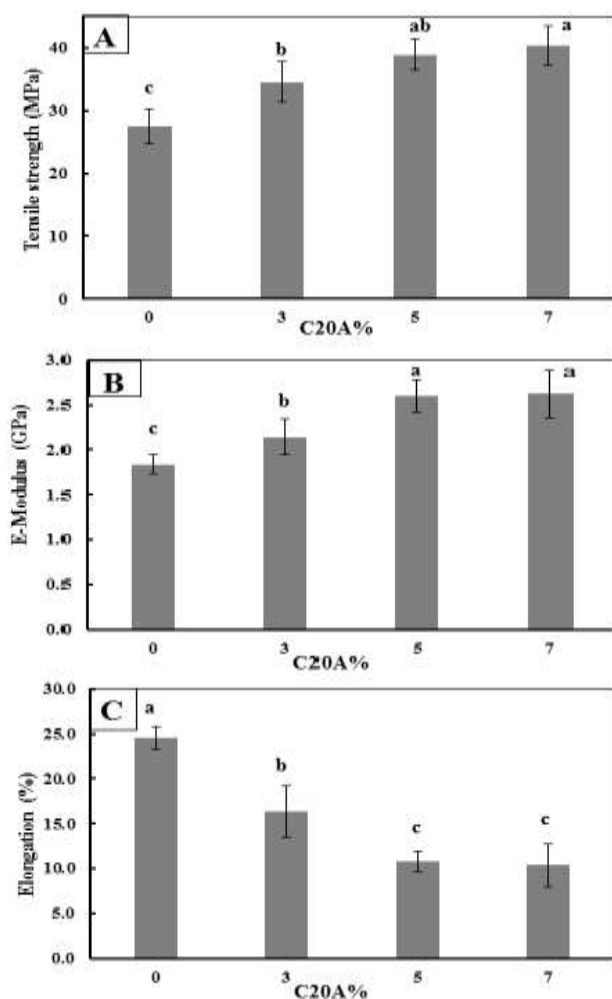


Figure 5. Mechanical properties: TS (A), E-M (B) and E% (C) of pure PLA and nanocomposites. *a,b,c*, Letters indicate the statistical difference (Same letters indicate no significant differences and different letters indicate significant differences between columns.)

3.4. Thermal characteristics

Thermal analysis of PLA and its nanocomposites has of great importance in food packaging. Figure 6 shows the DSC graphs for both pure PLA and its nanocomposites undergoing heating up to 200°C. It should be noted that all samples were characterized by a glass transition temperature (T_g), melting peak (T_m) and their degree of crystallinity ($\chi\%$). The values obtained from all samples are tabulated in Table 2. T_g is the temperature at which the material undergoes a structural transition from an amorphous solid state (glassy state) to a more viscous (rubbery) state [37]. According to the Figure 6 the temperature of the endothermic peak is considered for all samples to be the T_g of samples and at T_g there is a step-like change, which is due to enthalpy relaxation. The pure PLA is characterized by a T_g at 53.83°C, a T_m at 153.95°C and finally $\chi\%$ of 41.36. With increasing C20A content from 0 to 3, 5 and 7 percentages, T_g increased to 57.55, 59.16 and 60.48°C respectively. In all nanocomposites, lower mobility of PLA chains, due to their interactions with silicate surface, causes an increase in the T_g . So, the maximum increase was observed for 7 percentage of C20A contents. It seems that silicate aggregates were efficiently dispersed under the used blending conditions at higher C20A contents.

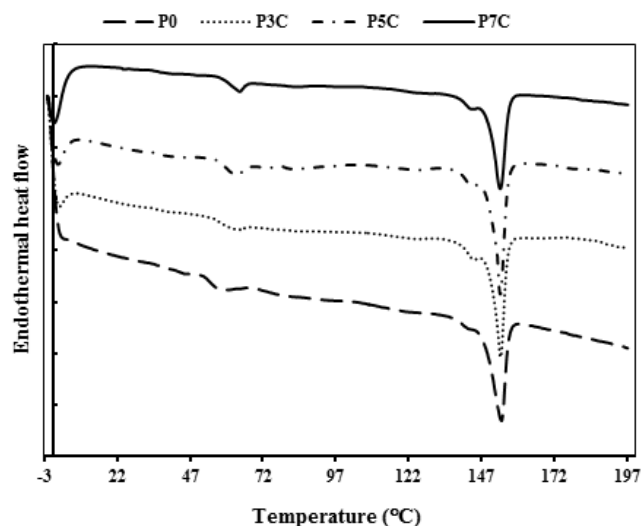


Figure 6. DSC graphs of pure PLA and nanocomposites

Table 2. Thermal characteristics of the samples evaluated as determined by DSC

Composition	T _g (°C)	T _m (°C)	χ%
PLA	53.83	153.95	41.36
PLA/3%C	57.55	153.47	44.82
PLA/5%C	59.16	153.47	47.52
PLA/7%C	60.48	153.51	48.05

All T_m values were similar in the range of 153.47°C for nanocomposites with 3 and 5 percentage of C20A to 153.95 °C for pure PLA. This indicated that the incorporation of C20A into PLA (97/3; 95/5; and 93/7) did not affect the T_m.

It is clear that the crystallinity of the PLA matrix increased with increasing the amount of the C20A. The degree of crystallinity increased from 41.36% (neat PLA) to 48.05% (7% of C20A). This behavior can be explained by the assumption that silicate layers act as efficient nucleating agents that enhance the crystallization of polymers molecules [28]. It was shown by Nam et al. (2003) [38] and Ray et al. (2003) [39] that large surface area of the exfoliated clays facilitates the PLA crystallization process.

3.5. Water vapor permeability

Since water is one of the most important causes of food spoilage reactions, water vapor transmission rate (WVTR) and Water vapor permeability (WVP) of food packaging materials, especially bio-polymers, are the most important characteristics. WVTR and WVP of polymeric films depend on hydrophilic and hydrophobic nature of materials, manufacturing process, type and the amount of additives, the incorporation method of additives, exist of pores, cracks and tortuosity in film and finally the order in the polymer structure [40]. WVP of nanocomposite films compounded with organically modified nanoclays, i.e., C20A, decreased, while that of films composited with unmodified natural nanoclay, CNa⁺, increased slightly. This result is mainly attributed to the hydrophobicity of organically modified nanoclays and hydrophilicity of unmodified nanoclay [19, 41, 42, 43].

Table 3 and Figure 7 show WVP values of PLA and PLA-based nanocomposite films. The

Table 3. Water Vapor Permeability (WVP) of pure PLA nanocomposites containing C20A

Composition	WVP * E-11 (g/m.s.Pa)
PLA	1.87 ± 0.11 ^a
PLA/3%C	1.63 ± 0.21 ^b
PLA/5%C	1.39 ± 0.13 ^c
PLA/7%C	0.92 ± 0.18 ^d

^{a,b,c,d} Letters indicate the statistical difference in column, (between samples)

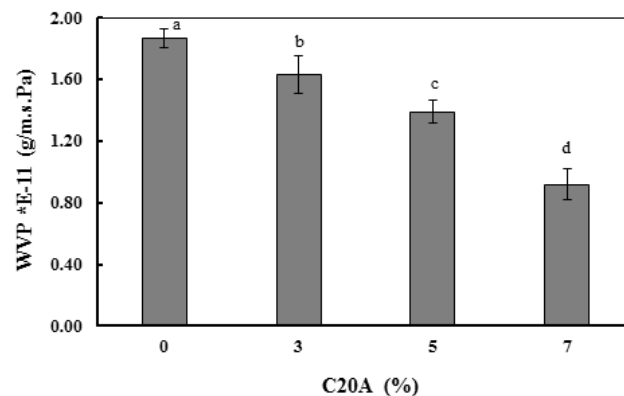


Figure 7. Effect of C20A content (%) on WVP of PLA nanocomposites. ^{a,b,c,d} Letters indicate the statistical difference (Same letters indicate no significant differences and different letters indicate significant differences between columns.)

WVP of nanocomposite films changed significantly ($P < 0.05$) depending on the C20A content. The WVP was $1.87 \cdot 10^{-11}$ g/m.s.Pa for pure PLA, that was in good agreement with WVP reported ($1.89 \cdot 10^{-11}$ g/m.s.Pa) by Auras et al. (2003) [44], for PLA film made with nominally 98% L-lactide. WVP decreased to $1.63 \cdot 10^{-11}$, $1.39 \cdot 10^{-11}$ and $0.92 \cdot 10^{-11}$ g/m.s.Pa for the nanocomposite films containing 3, 5 and 7% of C20A, respectively. In other words, incorporation of 3-7% of nano-clay to polymer matrix, led to 12-50% decrease in their permeability to water vapor. The improvement of water vapor barrier properties of polymer/clay composite films comparing to pure PLA films is mainly attributed to the tortuous path for water vapor diffusion due to the impermeable clay layers distributed in polymer matrix consequently increasing the effective diffusion path length. The tortuous path theory is based on the premise that a molecule must follow a more complicated path when nanoclay is dispersed throughout the polymer matrix than when the matrix consists of the homopolymer alone. The

shape and state of exfoliation/intercalation of the platelets and their orientation in the polymer matrix can also influence the degree of tortuosity [41, 42, 43].

3.6. Film microstructure

The microstructural study of the nanocomposites gives relevant information about the arrangement of the components, allowing us a better understanding of water vapor transmission mechanisms and mechanical properties [24].

With the aim of evaluating particles dispersion and particle/polymer interfacial adhesion, the freeze-fracture surfaces of pure PLA and its nanocomposites with C20A, have been observed by SEM. As can be seen in Figure 8, pure PLA has a uniform structure with holes and cracks, which confirm the high WVP of this biopolymer. Micrographs of the nanocomposites showed a good distribution and interfacial adhesion of nanoparticles in polymer matrix, so that the cluster structures could not be seen. Also with increasing the content of nanoparticles, nanocomposite structure became more closed.

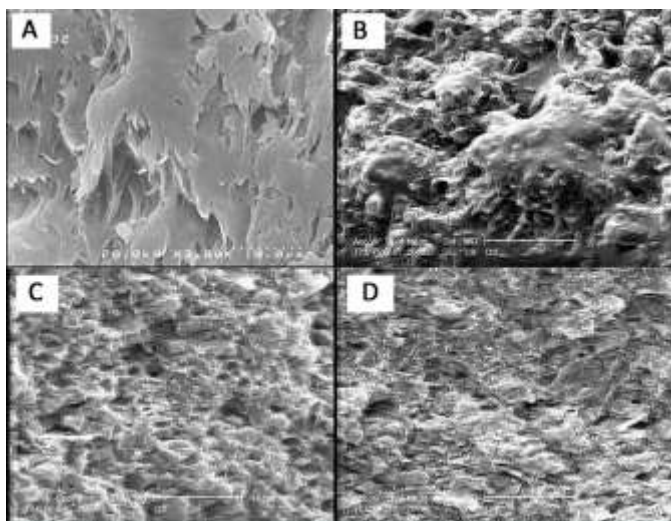


Figure 8. SEM images of freeze-fracture surfaces of A: pure PLA, B: 3%C20A, C: 5%C20A and D: 7%C20A

3.7. Atomic force microscopy

The atomic force microscopy (AFM) technique is a powerful tool for studying surfaces and has been used to provide qualitative and quantitative

information about biopolymers at the nanometer scale that are often inaccessible by any other experimental technique [45, 46].

Figure 9 shows 3D images of pure PLA and its nanocomposite containing 5% C20A; the corresponding results of roughness parameters are shown in Table 4. Comparison of images and table data indicates that with the incorporation of nanoparticles into the polymer, polymers smooth surface became rough. Roughness parameters, including S_a , S_q and S_{dq} , for pure PLA were: 34.00 nm, 44.90 nm and 0.076, respectively, while these values increased to 117.50 nm, 151.50 nm and 0.163 by adding nanoparticles. According to these results and the significant effect of 5% C20A on the surface roughness of the films, with increasing C20A content to 7%, more changes in the surface roughness should be seen. About the sample with 3% C20A, due to the small amount of nanoparticles, roughness values would be less.

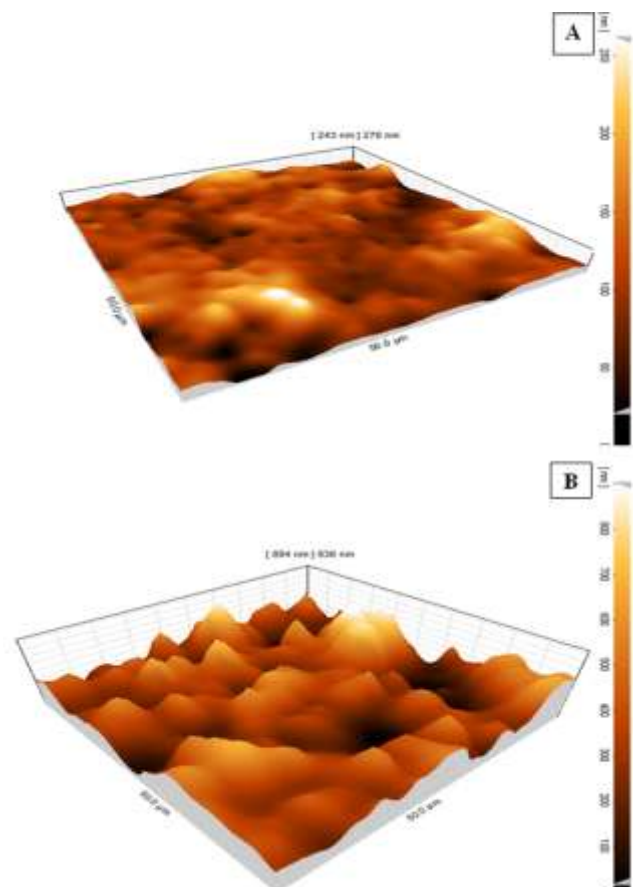


Figure 9. AFM topographic images of the neat PLA (A), PLA/5%C20A (B)

Table 4. Roughness parameters obtained from atomic force microscopy images

Composition	Roughness parameters		
	S _a (nm)	S _q (nm)	S _{dq}
PLA	34.00 ± 2.12 ^b	44.90 ± 1.70 ^b	0.076 ± 0.001 ^b
PLA/5%C	117.50 ± 4.95 ^a	151.50 ± 2.32 ^a	0.163 ± 0.011 ^a

^{a,b} Letters indicate the statistical difference in column, (between samples)

4. CONCLUSIONS

Biodegradable polymer/layered silicate nanocomposite films with 3, 5 and 7 % of C20A were prepared by solution casting using chloroform as the solvent. Physical properties including: thickness, transparency and apparent colors, Showed minor changes with increasing of C20A load. XRD study was performed in order to investigate the intercalation and exfoliation status of clay by incorporating of polymers in prepared nanocomposite film, which referred to that the specific peak of clay moved to the lower degrees and the clay nanolayer formed an intercalated structure. This result confirms the diffusion of polymer chains inside galleries of clay. Generally, the TS and E-M of the films increased and E decreased with increasing the concentration of C20A. DSC analysis on nanocomposites containing increasing levels of C20A indicated that there was no significant change on T_m , while T_g and $\chi\%$, increased significantly with the incorporation of nano-clay which is attributed to the lower mobility of PLA chains due to their interactions with the nanoclay surface and function of nanoclay as efficient nucleating agent. It was confirmed that water vapor permeabilities of PLA/C20A showed a high degree of improvement and decreased because the tortuosity of permeable channel increased with increasing the content of clay. SEM micrographs showed that most of the nanoclay layers were separated from each other and dispersed homogeneously in PLA matrix and also had good interaction with the polymer matrix. Finally, AFM surface analysis indicated that the surface roughness of the films was affected by the addition of C20A, and it became rougher.

ACKNOWLEDGEMENT

This research was supported by the Research and

Development Corporation of Zamzam CO.

REFERENCES

1. A.R. McLauchlin and N.L. Thomas: Polym. Degrad. Stabil., Vol. 94, (2009), pp. 868–872.
2. J.R. Dorgan, H.J. Lehermeier, L.I. Palade and J. Cicero: Macromol. Symp., Vol. 175, (2001), pp. 55–66.
3. J.M. Krochta and C.D. Mulder-Johnston: Food. Tech., Vol. 51, (1997), pp. 61–74.
4. C.C. Chen, J.Y. Chueh, H. Tseng, H.M. Huang and S.Y. Lee: Biomaterials., Vol. 24, (2003), pp. 1167–1173.
5. B. Li and M. Yang: Polym. Polym. Compos., Vol. 17, (2006), pp. 439–443.
6. G. Bhuvanesh, R. Nilesh and H. Jons: Prog. Polym. Sci., Vol. 32, (2007), pp. 455–82.
7. A.P. Gupta and V. Kumar: Eur. Polym. J., Vol. 43, (2007), pp. 4053–74.
8. M.F. Chiang, E.C. Chen and T.M. Wu: Polym. Degrad. Stabil., Vol. 97, (2012), pp. 995–1001.
9. S.Y. Gu, M. Yang, T. Yu, T.B. Ren and J. Ren: J. Polym. Int., Vol. 57, (2008), pp. 982–6.
10. J. Lunt: Polym. Degrad. Stabil., Vol. 59, (1998), pp. 145–51.
11. R.P. Singh, J.K. Pandey, D. Rutot, P.h. Degee and P.h. Dubois: Carbohydr. Res., Vol. 338, (2003), pp. 1759–1769.
12. S. Solarski, M. Ferreira, E. Devaux, G. Fontaine, P. Bachelet, S. Bourbigot, R. Delobel, Ph. Coszach, M. Murariu and F.A. Da Silva: J. Appl. Polym. Sci., Vol. 109, (2008), pp. 841–51.
13. Arora and G.W. Padua: J. Food. Sci., Vol. 75, (2010), pp. 43–49.
14. R.M. Rasal, A.V. Janorkar, D.E. Hirt: Prog. Polym. Sci., Vol. 35, (2010), pp. 338–356.
15. M. Zenkiewicz and J. Richert: Polym. Test., Vol. 27, (2008), pp. 835–840.
16. Usuki, Y. Kojima, A. Usuki, M. Kawasumi, A. Okada, Y. Fukushima, T. Kurauchi and O. Kamigaito: J. Mater. Res., Vol. 8, (1993), pp. 1185–9.
17. M. Pluta, A. Galeski, M. Alexandre, M.A. Paul and P. Dubois: J. Appl. Polym. Sci., Vol. 86, (2002), pp. 1497–506.

18. B. Harinatharavimal, H. Azman, U.W. Mat, A.A. Yussuf and A.S.B. Razak: *Mater. Design.*, Vol. 31, (2010), pp. 3289-3298.
19. J.W. Rhim, S.I. Hong and C.S. Ha: *LWT-Food. Sci. Technol.*, Vol. 42, (2009), pp. 612-617.
20. J.W. Rhim, K.A. Mohanty, S.P. Singh and P.K.W. Ng: *J. Appl. Polym. Sci.*, Vol. 101, (2006), pp. 3736-3742.
21. E.W. Fisher, H.J. Sterzel and G. Wegner: *Kolloid-Zeitschrift and Zeitschrift Fur Polymer.*, Vol. 25, (1973), pp. 980-82.
22. ASTM, D882-91. *Tensile Testing of Thin Plastic Sheeting*, American Society for Testing and Materials, Philadelphia, PA, (1996).
23. ASTM, E96-05. *Standard Test Methods for Water Vapor Transmission of Materials*, American Society for Testing and Materials, Philadelphia, PA, (1995).
24. M. Ghasemlou, F. Khodaiyan and A. Oromiehie: *Carbohydr. Polym.*, Vol. 84, (2011), pp. 477-483.
25. Gennadios, C.L. Weller and C.H. Gooding: *J. Food. Eng.*, Vol. 21, (1994), pp. 395-409.
26. Q.H. Zeng, A.B. Yu, G.Q.M. Lu and D.R. Paul: *J. Nanosci. Nanotechnol.*, Vol. 5, (2005), pp. 1574-1592.
27. H.C. Koh, J.S. Park, M.A. Jeong, H.Y. Hwang, Y.T. Hong, S.Y. Ha and S.Y. Nam: *Desalination.*, Vol. 233, (2008), pp. 201-209.
28. L.H. Lin, H.J. Liu and N.K. Yu: *J. Appl. Polym. Sci.*, Vol. 106, (2007), pp. 260-266.
29. J.H. Lee, T.G. Park, H.S. Park, D.S. Lee, Y.K. Lee, S.C. Yoon and J.D. Nam: *Biomaterials.*, Vol. 24, (2003), pp. 2773-8.
30. L. Jiang, J. Zhang and M.P. Wolcott: *Polymer.*, Vol. 48, (2007), pp. 7632-44.
31. M. Alexandre and P. Dubois: *Mat. Sci. Eng. R.*, Vol. 28, (2000), pp. 1-63.
32. J.K. Pandey, A.P. Kumar, M. Misra, A.K. Mohanty, L.T. Drzal and R.P. Singh: *Nanotechnol.*, Vol. 5, (2005), pp. 497-526.
33. S. Pavlidou, C.D. Papaspyrides: *Prog. Polym. Sci.*, Vol. 33, (2008), pp. 1119-1198.
34. R.S. Sinha and M. Bousmina: *Prog. Mater. Sci.*, Vol. 50, (2005), pp. 962-1079.
35. J.W. Rhim: *Carbohydr. Polym.*, Vol. 86, (2011), pp. 691-699.
36. H. Alamsi, B. Ghanbarzadeh and A.A. Entezami: *Int. J. Biol. Macromol.*, Vol. 46, (2010), pp. 1-5.
37. B. Ghanbarzadeh and A.R. Oromiehi: *J. Food. Eng.*, Vol. 90, (2009), pp. 517-524.
38. J.Y. Nam, S.S. Ray and M. Okamoto: *Macromolecules.*, Vol. 36, (2003), pp. 7126-7131.
39. S.S. Ray, K. Yamada, M. Okamoto and K. Ueda: *Polymer.*, Vol. 44, (2003), pp. 857-866.
40. M.B. Vasconez, S.K. Flores, C.A. Campos, J. Alvarado and L.N. Gerschenson: *Food. Res. Int.*, Vol. 42, (2009), pp. 762-769.
41. K. Yano, A. Usuki and A. Okai: *J. Polym. Sci. Pol. Chem.*, Vol. 35, (1997), pp. 2289-2294.
42. E.L. Cussler, S.E. Highes, W.J. Ward and R. Aris: *J. Membrane. Sci.*, Vol. 38, pp. (1998), 161-174.
43. C. Thellen, C. Orroth, D. Froio, D. Ziegler, J. Lucciarini, R. Farrell, N.A. D'Souza and J.A. Ratto: *Polymer.*, Vol. 46, (2005), pp. 11716-11727.
44. R. Auras, B. Harte, S. Selke and R. Hernandez: *J. Plast. Film. Sheet.*, Vol. 19, (2003), pp. 123-35.
45. C. Elofsson, P. Dejmek, M. Paulsson and H. Burling: *Int. Dairy. J.*, Vol. 7, (1997), pp. 813-819.
46. B. Ghanbarzadeh, A.R. Oromiehie, M. Mousavi, P.M. Falcone, Z. Emam D-Jomeh and E.R. Rad: *Packag. Technol. Sci.*, Vol. 20, (2007), pp. 155-163.
47. D. Lewitus, S. McCarthy, A. Ophir and S. Kenig: *J. Polym. Environ.*, Vol. 14, (2006), pp. 171-177.